Inductive measurement of ultrafast magnetization dynamics in thin-film Permalloy

T. J. Silva[a] and C. S. Lee
National Institute of Standards and Technology, Boulder, Colorado 80303

T. M. Crawford[b] and C. T. Rogers
Department of Physics, University of Colorado, Boulder, Colorado 80309

(Received 17 August 1998; accepted for publication 26 February 1999)

An inductive technique for the measurement of dynamical magnetic processes in thin-film materials is described. The technique is demonstrated using 50 nm films of Permalloy ($Ni_{81}Fe_{19}$). Data are presented for impulse- and step-response experiments with the applied field pulse oriented in the plane of the film and transverse to the anisotropy axis. Rotation times as short as 200 ps and free oscillations of the magnetization after excitation are clearly observed. The oscillation frequency increases as the dc bias field parallel to the anisotropy axis increases as predicted by classical gyromagnetic theory. The data are fitted to the Landau–Lifshitz equation, and damping parameters are determined as a function of dc bias field. Damping for both impulse and step excitations exhibits a strong dependence on bias field. Damping for step excitations is characterized by an anomalous transient damping which rapidly increases at low dc bias field. Transformation of the data to the frequency domain reveals a higher order precessional mode which is also preferentially excited at low dc bias fields. A possible source for both phenomena is precessional mode saturation for large peak rotations. The technique has the potential for 20 ps resolution, although only 120 ps resolution is demonstrated due to the limited bandwidth of the waveguides used. © *1999 American Institute of Physics.* [S0021-8979(99)06111-3]

I. INTRODUCTION

Rapid increases in the areal density of hard disk data storage systems over the last decade have resulted in a commensurate increase in the data rate of the magnetic recording channel. Extrapolation from recent trends in disk drive performance predicts data rates approaching 1 GHz by the middle of the next decade.[1] This increase has fueled concern about the fundamental limits to the speed of the magnetic components in disk drive systems. In this paper, we describe a technique for measuring the high-speed magnetic response of thin films, and report response times for $Ni_{81}Fe_{19}$ (Permalloy), a magnetic alloy used throughout the data storage industry for recording heads. We have observed magnetic rotations of nearly 90° in a characteristic time of 200 ps for an applied transverse field of 1.7 kA/m (21 Oe).

It has been known since the early 1960s that fast switching speeds of <1 ns could be achieved in thin films of Permalloy. Dietrich, Proebster, and Wolf were the first to measure switching speeds of 1 ns using an inductive technique.[2,3] When field impulses were applied transverse to the easy axis of the film, oscillations in the inductive signal, indicative of underdamped magnetic precession, were observed.[4] This inductive approach used the discharge of a 50 Ω charge line through a coaxial mercury relay as a pulsed current, and therefore pulsed magnetic field source. Resulting pulse widths were less than 350 ps, although an exact determination was limited by the temporal resolution of the existing sampling technology. Strip transmission lines were used to deliver the electromagnetic field pulse to the sample, and pickup coils were positioned around the transmission lines to detect the inductive signal from the changing magnetization in the sample. The dynamics were partially obscured by the coupling of the incident microwave pulse to the inductive pickup coil. To extract the dynamic magnetization response, wave forms were measured with and without an applied saturating magnetic field and subsequently subtracted.

We describe an inductive method for the measurement of ultrafast magnetic phenomena in thin-film materials which advances the work of Dietrich *et al.* in four important ways. First, a time-domain transmission geometry which avoids the need for inductive pick-up coils is used. Second, lithographically patterned coplanar waveguides are used to deliver field pulses to the magnetic films. Various field-to-voltage ratios can be obtained by patterning the waveguides to different widths. Lower voltage solid-state microwave pulse and step sources may be employed by using 100 μm and narrower stripline widths. Third, modern pulse/step sources are capable of much faster rise times than can be obtained from mercury reed relays. Fourth, wave form subtraction is accomplished digitally and employs digital signal processing to improve signal-to-noise ratios.

II. METHOD

A. Experimental apparatus

In Fig. 1, we present a schematic representation of the experimental arrangement. Several different sources are used

[a]Electronic mail: silva@boulder.nist.gov
[b]Present address: NIST, Boulder, CO 80303.

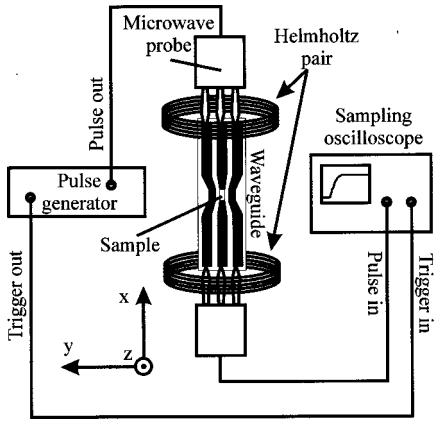

FIG. 1. Diagrammatic sketch of experimental configuration.

for pulse generation. For producing *impulses*, we use a commercial InGaAs photodiode driven by optical pulses from a mode-locked Ti:sapphire laser. We operate the photodiode at bias voltages approaching $-50\,\mathrm{V}$. The diode acts as a photoconductive switch when using 50 fs optical pulses with roughly 10 nJ of energy, limited principally by the capacitance of the diode and the carrier drift velocity. The resultant electrical pulses have amplitudes of 5 V, rise times of 80 ps, and pulse widths of 200 ps, and arrive at a frequency of 100 MHz which is set by the laser repetition rate.

To produce magnetic field *steps* we use a commercial solid-state pulse generator. Pulses from this source have amplitudes of 10 V, rise times of 50 ps, and pulse widths of 10 ns, and arrive at a frequency of 1 MHz. Trigger jitter for the commercial pulse generator is less than 5 ps (rms). The voltage pulse is delivered to the coplanar waveguide with high-bandwidth coaxial cable. Insertion onto, and extraction from, the waveguide is accomplished with $50\,\Omega$ triaxial microwave probes. Each probe has an insertion loss of $<0.3\,\mathrm{dB}$ ($\sim 4\%$) at 7 GHz.

Coplanar waveguides were lithographically fabricated on single-crystal (100) GaAs substrates with resistivity in excess of $16\times10^{7}\,\Omega\,\mathrm{cm}$, using 750 nm thick Au conductive strips. GaAs was chosen for its high dielectric constant ($\varepsilon_r = 13.1$) and low loss tangent. To maximize the usable bandwidth of the structure, we have sought to minimize conductor losses. For Au at 20 GHz, the skin depth is calculated to be 2 μm. Our deposition system limits us to a maximum thickness of 0.75 μm, which causes some attenuation of the highest frequency components, but is adequate for the purposes of this work.

The waveguide for impulse–response measurements has a 100 μm width along its entire length. The waveguide for step-response measurements has a 100 μm center conductor width at the two ends and tapers to 50 μm in the middle for a length of 1 mm. The total waveguide length is 50 mm in both cases. The waveguide was designed to be $50\,\Omega$ using conventional design criteria for coplanar waveguides with finite-width ground planes.[5] A nominally 50 nm thick $Ni_{81}Fe_{19}$ (Permalloy) film was deposited and subsequently lithographically patterned onto the waveguide structure along the entire 1 mm segment in the center of the waveguide for both the impulse and step response measurements, in a geometry similar to that employed by Freeman *et al.* for time-resolved magneto-optic studies of magnetic reversal in Permalloy films.[6] The Permalloy films were grown by dc magnetron sputtering with 0.27 Pa (2×10^{-3} Torr) argon pressure at 300 W. A uniaxial anisotropy axis oriented parallel to the waveguide was induced in the Permalloy film by application of a magnetic field during film growth. A planarization layer of 1 μm thickness composed of photosensitive polymer between the Au and NiFe films was necessary to achieve the desired coercivity and anisotropy for the magnetic layer.

The NiFe bulk magnetic properties were measured on codeposited NiFe coupons. Using a *B-H* looper, we measured an easy axis coercivity of 80 A/m (1.0 Oe), with 0.99 loop squareness (ratio of remanent to saturation magnetization, M_r/M_s). In the hard direction, we measured a uniaxial magnetocrystalline anisotropy H_k^{xtal} of 344 A/m (4.3 Oe). M_s was measured to be 840 kA/m ($840\,\mathrm{emu/cm^3}$) using a superconducting quantum interference device (SQUID) magnetometer to determine the perpendicular shape anisotropy, $H_{k,\perp}^{s}=M_s$. Film thickness δ was then deduced to be 47 ±1 nm by measuring the absolute moment of the coupon.

The 50 μm wide sample was imaged by wide-field Kerr microscopy to ascertain the domain structure of the patterned film. The structure was single domain in the middle of the stripe only for bias field $H_b>80\,\mathrm{A/m}$ (1 Oe). For smaller bias fields, the magnetization broke into a four-domain structure, with triangular closure domains at the two ends of the stripe and two oppositely oriented longitudinal domains throughout the length of the stripe. The triangular closure domains remained present for fields in excess of 800 A/m (10 Oe).

The waveguide bandwidth was 10 GHz (3 dB point) before deposition of the planarization and magnetic layers. The completed waveguide has a bandwidth of 2.5 GHz, as measured by both a calibrated network analyzer and time-domain transmissivity. We attribute the reduction in bandwidth to the polymeric buffer layer. The actual characteristic impedance Z_0 was 60 Ω, resulting in some impedance mismatch between the waveguide and microwave probes. This mismatch is primarily due to the nonzero dc resistance of the center conductor stripe ($\approx 20\,\Omega$). The coaxial cables employed have a bandwidth of ~ 3 GHz. Thus, the time resolution of the present implementation is limited to 140 ps.

The transmitted pulse is detected by a high-speed sampling oscilloscope with an 18 GHz bandwidth. A trigger pulse for the sampling oscilloscope is derived from the pulse generator. Sampling intervals are 9.7 ps, resulting in 512 samples over a 5 ns trace. A Helmholtz coil pair, calibrated with a Hall probe, is used to apply a variable longitudinal bias field to the sample with a magnitude as large as 4 kA/m (50 Oe) in a direction parallel to the easy axis of the sample.

The sampling oscilloscope has a raw input noise of ~ 1 mV (rms) over the full 18 GHz bandwidth. By averaging 4096 sampled wave forms, we can reduce the noise level to 16 μV (rms). The digitized wave forms are stored in 16 bit memory, with a discretization of 15 μV, matching the noise of the instrument. To avoid damage to the sensitive electron-

ics of the instrument, we reduce the input from the pulse generator with high-bandwidth attenuators. For a 10 V pulse, at least 20 dB of attenuation must be used, and for this case, the resulting noise level of the instrument is 160 μV (rms), referenced to the point before the SMA attenuators. After averaging, the final acquired wave form is transferred digitally to a computer for processing and analysis.

With the magnetic sample saturated by a large transverse field >4 kA/m (50 Oe) in the direction of the pulsed field, a reference wave form in which no magnetic activity has occurred is acquired. The transverse field is provided by either Helmholtz coils (not shown in Fig. 1) or a hand-held permanent magnet, with identical results. This reference wave form is subsequently subtracted from other acquired wave forms, allowing the observation of precessional effects. One systematic source of error arises from the fact that small temporal drifts in the triggering point of the wave forms can substantially corrupt the processed data. As an example, a 100 fs drift in the trigger point between the reference and inductive wave forms can produce a spurious 20 mV spike, which is temporally coincident with the rising edge of the unprocessed wave forms. To remove this time shift, we developed a computational algorithm which maximizes the temporal correlation of the first 40 ps of the rising edges of the two wave forms. The wave forms are then interpolated to allow for temporal shifts smaller than the sampling interval.

B. Induced voltage signal

The inductive voltage signal V_p may be related to the sample magnetization in the transverse direction through Faraday's law. We use reciprocity to derive such a relation, greatly simplifying the calculation. Reciprocity, in its most general form, states that the inductive coupling between two flux linkages is independent of which linkage is actually being driven by a current.[7] For this specific case, reciprocity dictates that the field profile of the waveguide for a unit excitation current may be substituted for the waveguide's spatial sensitivity to changing magnetization. We assume that the sample magnetization lies primarily in the x-y plane, and that it is uniform in the x direction. (See Fig. 1 for coordinate axes.) Thus, we ignore the sensitivity of the waveguide to perpendicular magnetization and treat the problem as one dimensional along the y direction. (Further justification for these assumptions is presented at the end of Sec. III.) The magnetic field in the y direction produced by a current I at a distance z above the waveguide is represented by $H_y(I;y,z)$, where the y axis is transverse to the direction of current. At a position close to the center conductor of the waveguide but far from an edge, the center conductor appears as an infinite sheet of current, which produces a field of $I/2w$. Far from the center conductor, the functional form of the field requires a solution to Laplace's equation with the proper boundary condition.

The Karlqvist equations for the fields above a two-dimensional, gapped recording head are derived with a boundary condition of linearly increasing potential across the gap width.[8] This boundary condition is identical to that of a uniform current strip, where the gap between the high-permeability head material at $z=0$ is replaced with the current strip.[9] Solving with these boundary conditions leads to a transverse field given by

$$H_y(I;y,z)=\frac{1}{\pi}\frac{I}{2w}\left[\arctan\left(\frac{(w/2)+y}{z}\right)+\arctan\left(\frac{(w/2)-y}{z}\right)\right]. \tag{1}$$

$H_y(I;y,z)$ is within 90% of its maximum field value of $I/2w$ at a distance of $3.1z$ from the waveguide edge, or only 5% of the total center conductor width for $z=0.75\,\mu$m and $w=50\,\mu$m. Thus, we may approximate $H_y(I;y,z)$ for $z\ll w$ as

$$H_y(I;y,z)=\frac{I}{2w}f(z,w)[u(y+w/2)-u(y-w/2)], \tag{2}$$

where $u(y)$ is the Heaviside step function and $f(z,w)$ is a function which accounts for the loss of field due to the nonzero spacing. The spacing loss function $f(z,w)$ is approximated by determining the amplitude of the function described by Eq. (2) which has the same integrated value across the width of the sample as that of Eq. (1). In this treatment, we have ignored the field produced by current in the ground planes since that field is primarily perpendicular to the sample plane and is too weak to cause **M** to tip out of plane.

From reciprocity, the flux that winds around the waveguide center conductor from a magnetic sample of thickness δ, length l, and width w may be calculated as[7,10]

$$\begin{aligned}\Phi&=\frac{\mu_0}{I}\int\int\int_{\text{sample}}H_y(I;x,y,z)M_y(x,y,z)\,dx\,dy\,dz\\&=\frac{\mu_0}{2w}l\,\delta f(z,w)\int_{-w/2}^{+w/2}M_y(y)\,dy\\&=\frac{1}{2}\mu_0\overline{M_y}l\,\delta f(z,w).\end{aligned} \tag{3}$$

We have assumed that the magnetization is uniform over the thickness and along the length of the sample. An inductive voltage is produced by the change in flux, $V=-d\Phi/dt$. The inductive voltage pulse within the waveguide is bipolar. The induced current is $I=V/(2Z_0)$, since each leg of the waveguide provides Z_0 of series resistance. This results in two pulses of equal amplitude but of opposite polarity with magnitude $V_p=\frac{1}{2}V=-\frac{1}{2}d\Phi/dt$, traveling in opposite directions within the waveguide. Only the one pulse which travels in the same direction as the driving voltage pulse is actually detected by the sampling oscilloscope. (A power splitter has been used to detect the second pulse which travels back toward the pulse generator, verifying its equal magnitude and opposite polarity.) Thus, our result from Eq. (3) is halved. If the waveguide has a nonzero dc resistance R_{dc}, this will act as an additional loss for the detected inductive pulse. After taking the time derivative, we have

$$V_p=\left(\frac{\mu_0 l\,\delta f(z,w)}{4}\right)\left(\frac{Z_0}{Z_0+\frac{1}{2}R_{\text{dc}}}\right)\frac{d\overline{M_y}}{dt}. \tag{4}$$

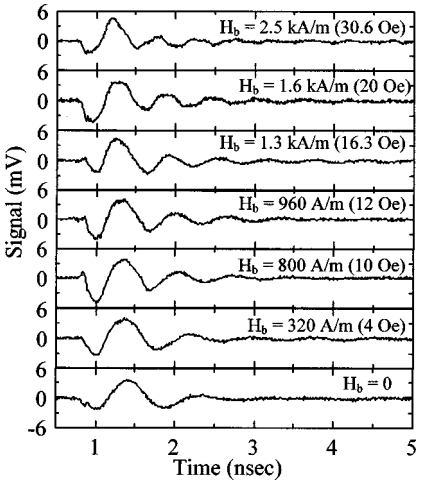

FIG. 2. Inductive wave forms obtained for impulse excitations with the 100 μm wide NiFe sample. Wave forms were acquired with different levels of dc bias field H_b applied along the easy axis of the sample.

By integrating the measured voltage pulse, we can infer the average amount of magnetization that rotates

$$\overline{M_y}=\left(\frac{4}{\mu_0 l\,\delta f(z,w)}\right)\left(\frac{Z_0+\frac{1}{2}R_{\rm dc}}{Z_0}\right)\int V_p\,dt. \tag{5}$$

III. RESULTS

A. Impulse excitations

1. Data and fitting

Figure 2 contains processed data for *impulse* excitations. Pulse amplitudes are estimated to be 380 A/m (4.7 Oe). The different curves are for seven longitudinal bias fields ranging from 0 to 2.5 kA/m (30.6 Oe). One immediately notes the existence of free magnetic oscillations in the data, similar to those previously observed by Wolf.[4] The existence of inductive oscillations long after application of the field pulse, where the magnetic response is no longer driven, is characteristic of highly underdamped gyromagnetic precession. These data are well fitted to an exponentially damped sinusoid

$$\phi(t)=\beta_0\sin(\omega_p t+\varphi)e^{-t/\tau}, \tag{6}$$

where $\phi(t)$ is the in-plane magnetization angle and $\phi=0$ is the equilibrium position; φ is an arbitrary phase parameter.

In the limit $\phi(t)\ll 1$, Eq. (6) is an approximate solution to the Landau–Lifshitz (LL) equation.[11] In Fig. 3 we show the dependence of both the precessional frequency and the LL damping parameter λ upon H_b, where we use[4]

$$\lambda=2/\tau. \tag{7}$$

The damping parameter λ has SI units of s^{-1}. It is not identical to the original definition of the damping parameter $\lambda_{\rm cgs}$ used by both Wolf[4] and Smith[11] (see Appendix A). They are related as $\lambda=4\pi\lambda_{\rm cgs}$.

We expect the behavior of f_p to be governed by the usual ferromagnetic resonance (FMR) result for gyromagnetic precession[12]

$$\omega_p=\gamma\mu_0\sqrt{M_s(H_k+H_b)}, \tag{8}$$

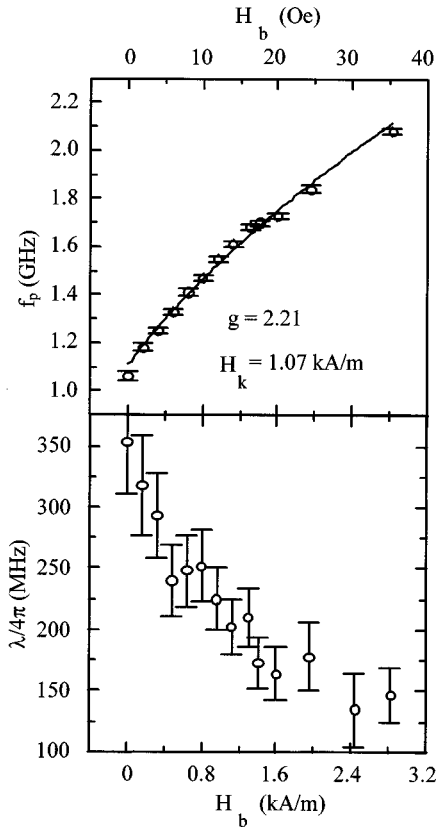

FIG. 3. Precessional frequency f_p and Landau–Lifshitz damping λ as a function of dc bias field H_b for the case of impulse excitations. The damping has been scaled by 4π to aid comparison with past published values of $\lambda_{\rm cgs}=\lambda/4\pi$ (see Appendix A). The solid curve drawn through the data for f_p is a fit to Eq. (8) with fitting parameters $g=2.21$ and $H_k=1.07$ kA/m.

where γ is the gyromagnetic ratio, H_k is the anisotropy field, and $(H_k+H_b)\ll M_s$. Fitting the precessional frequency $f_p=\omega_p/2\pi$ to the bias field produces fitted values for both H_k and the spectroscopic splitting factor g, where[12]

$$\gamma=\frac{g\mu_B}{\hbar}. \tag{9}$$

Here, μ_B is the Bohr magneton and $\hbar$ is Planck's constant $h/2\pi$. The fitted value of $g=2.21$ is only 6% greater than previously reported values for Permalloy.[13] H_k is 1.1 kA/m (14 Oe).

The hard-axis hysteresis loop was measured for the waveguide sample by Kerr optical techniques (nominally at the middle of the sample stripe) indicating a total static anisotropy of 1 kA/m (12.5 Oe). This anisotropy is significantly different from the measured value of 344 A/m (4.3 Oe) for the magnetocrystalline anisotropy. We presume that this additional anisotropy exhibited by the patterned structure arises from shape-induced demagnetizing effects. The relatively large anisotropy compared to the drive pulse amplitude, which results in small rotation angles, justifies the use of Eq. (6).

The increase in damping shown in Fig. 3 is qualitatively similar to that observed by Wolf, although we find that the average value of λ is about 40% greater.[4] Smith also observed a rapid increase in damping for 250 nm thick Permal-

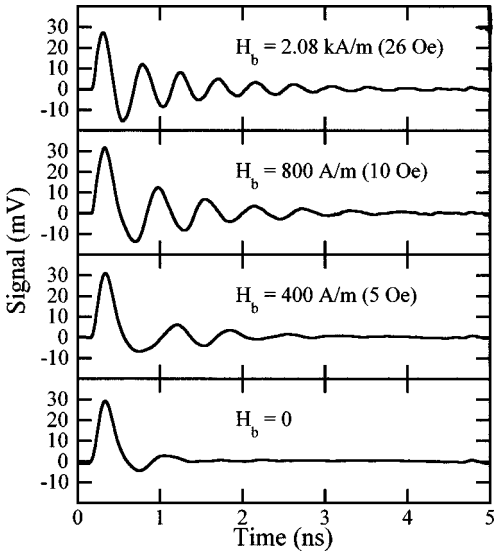

FIG. 4. Inductive wave forms obtained for step excitations with the 50 μm wide NiFe sample. Wave forms were acquired with different levels of dc bias field H_b applied along the easy axis of the sample. We infer an equilibrium magnetization rotation of $\sim 63°$ for $H_b=0$ from values of $H_p=1.6$ kA/m and $H_k=1.8$ kA/m fitted to the Landau–Lifshitz equation.

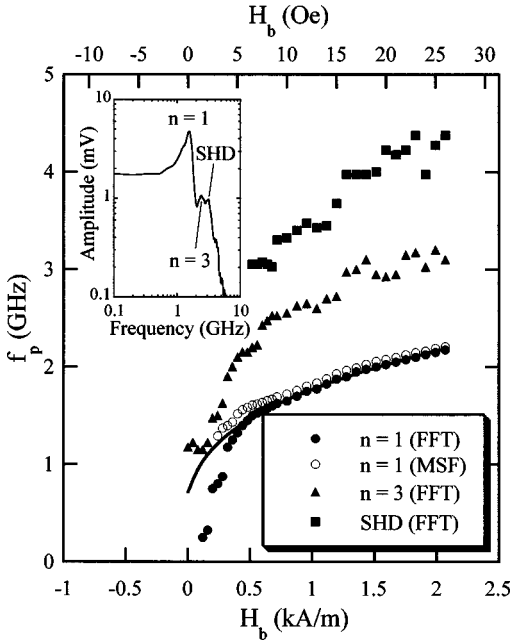

FIG. 5. Precessional frequency f_p as a function of dc bias field H_b for the case of step excitations, using both FFT and MSF analysis. Open circles are MSF results obtained by fitting the data using Eq. (11). All other data were obtained by identification of spectral peaks in Fourier transforms of the inductive data. Filled circles are believed to derive from the lowest order $n=1$ excitation. Filled squares are the second harmonic distortion of the $n=1$ mode. Filled triangles are a higher order precessional excitation, tentatively labeled $n=3$. The curve drawn through the lowest FFT spectral peak is a fit to Eqs. (12) and (15), with fitting parameters $g=2.21\pm0.02$ and $H_k=1.82\pm0.06$ kA/m (22.8 ± 0.8 Oe). The Fourier transform data were fit only for $H_b>440$ A/m (5.5 Oe). An inset shows one example of a Fourier transform spectrum for $H_b=0.6$ kA/m (7.5 Oe).

loy films measured by FMR when the resonance frequency is reduced. However, this increase becomes considerable only at frequencies below 500 MHz, whereas our data show a monotonic increase in damping from 2 GHz downward.[11] Such an increase in damping at reduced precessional frequencies typically has been ascribed to inhomogeneous line broadening caused by dispersion in H_k.[4,14–16]

B. Step excitations

1. Data

Several fully processed inductive wave forms for the case of *step* response are shown in Fig. 4. The four waveforms were acquired with different dc bias fields applied parallel to the easy axis of the film. A total of 1024 averages was used for each wave form. The applied bias field ranged from 0 to 2.1 kA/m (26 Oe). The step response data exhibit free inductive oscillations, similar to that observed for the impulse response data. The oscillations last almost 5 ns for the cases of 800 A/m and 2.08 kA/m bias fields. However, the free oscillations are greatly reduced in amplitude for zero bias field. Indeed, the wave forms for $H_b<400$ A/m (5 Oe) show only minor oscillations, indicative of critical damping. The full width at half maximum of the primary inductive pulse for $H_b=0$ is 200 ps.

2. Fitting

The magnetization can rotate to a relatively large equilibrium angle ϕ_0 for step response excitation. Nonetheless, we still expect the magnetization angle to evolve as an exponentially decaying sinusoid long after application of the step according to

$$\phi(t)=\phi_0+\beta_0\sin(\omega_p t+\varphi)e^{-t/\tau}, \tag{10}$$

similar to Eq. (6) for impulse response. Equation (10) is derived in Appendix A.

Keep in mind that inductive detection senses only the transverse component of magnetization $M_y=M_s\sin\phi(t)$. This fact will generally result in second-harmonic distortion (SHD) in the detected wave form since $\sin\phi$ far from $\phi=0$ is a nonlinear function. Fourier series expansions may be used to show that

$$\frac{dM_y}{dt}\approx\omega_p M_s\beta_0\left[\cos\phi_0\cos(\omega_p t+\varphi)e^{-t/\tau}-\frac{\beta_0}{2}\sin\phi_0\sin 2(\omega_p t+\varphi)e^{-2t/\tau}\right]+O(\beta_0^3), \tag{11}$$

where we have used the approximation $\beta_0 e^{-t/\tau}\ll 1$. Equation (11) and its more general form are derived in Appendix B. Large ϕ_0 will produce a second-harmonic distortion to the inductive signal which impedes a simple, damped sinusoidal fit. Indeed, a large magnetization rotation of $\phi_0=\pi/2$ will result in only a second-harmonic signal.

The modified sinusoidal fit (MSF) described by Eq. (11) was applied to the step response data to determine both f_p and τ, where $f_p=\omega_p/2\pi$. The data were fitted only after 2–3 cycles of oscillation to ensure that the motion of ϕ was small enough for the approximations used to derive Eq. (11) to be applicable. The results of fitting for f_p are shown in Fig. 5. The extracted damping constant λ is discussed below.

In addition to time-domain fitting, we may also determine the fundamental precession frequency by transforming the data to the frequency domain by a fast Fourier transform (FFT). Frequency spectra yield multiple peaks which are not apparent from the time-domain fitting to long-time behavior. We identify three different peaks from the spectra. The peak positions are continuous functions of H_b, all of which are plotted in Fig. 5 along with the results of the modified sinusoidal fit. A representative spectrum for the case of $H_b = 0.6\,\mathrm{kA/m}$ (7.5 Oe) is shown as an inset to Fig. 5, with all three spectral peaks identified. The frequency of the lowest spectral peak is nearly identical to that resulting from the MSF, suggesting that this peak results from the lowest order ($n=1$) precessional excitation. The highest frequency peak is attributed to the aforementioned SHD resulting from trigonometric distortion of the inductive signal because it occurs at exactly two times the frequency of the $n=1$ mode. In addition, a third peak, located at a frequency between the $n=1$ mode and the SHD, was also observed. We tentatively identify this peak as that of a higher-order $n=3$ precessional mode.

We expect f_p for the $n=1$ mode to approach the standard FMR result for weak damping:[11]

$$f_p = \frac{\gamma}{2\pi}\sqrt{\mu_0\left(\frac{\partial^2 U}{\partial \phi^2}\right)_{\phi_0}} \tag{12}$$

$$= \frac{\gamma\mu_0}{2\pi}\sqrt{M_s H_{\mathrm{eff}}(\phi_0)}, \tag{13}$$

$$H_{\mathrm{eff}}(\phi_0) = H_b\cos\phi_0 + H_p\sin\phi_0 + H_k\cos 2\phi_0, \tag{14}$$

where H_p is the field step amplitude, H_k is the uniaxial in-plane anisotropy, $U(\phi)$ is the free energy of the system, and ϕ_0 is the effective equilibrium direction of magnetization with respect to the longitudinal axis long after application of the field step. H_{eff} is the stiffness field; we have assumed negligible damping ($\lambda \ll f_p$). We call ϕ_0 an effective equilibrium direction only because it is not actually independent of position within the sample. However, $H_{\mathrm{eff}}(\phi_0)$ must be invariant with position for f_p to be a well-defined quantity of a precessional mode; that is, f_p must also be invariant with position as required for an eigenmode.

Since H_k is not known *a priori*, we must solve Eq. (12) simultaneously with the minimum energy criterion[17]

$$\left(\frac{\partial U}{\partial \phi}\right)_{\phi_0} = H_k\sin\phi_0 + H_b\tan\phi_0 - H_p = 0 \tag{15}$$

to numerically fit the data in Fig. 5. The solid line drawn through the FFT data is such a fit, with $g = 2.21 \pm 0.02$ and $H_k = 1.82 \pm 0.06\,\mathrm{kA/m}$ (22.8 ± 0.8 Oe). We also fitted the frequencies obtained from the modified sinusoidal fitting, with $g = 2.20 \pm 0.02$ and $H_k = 2.08 \pm 0.06\,\mathrm{kA/m}$ (26.0 ± 0.8 Oe). The fitted gyroscopic splitting factors are in excellent agreement with the value obtained from the impulse experiment.

We were forced to restrict the fit of the FFT data to $H_b \geqslant 440$ A/m (5.5 Oe); the fitting function and data diverge sharply for $H_b < 440$ A/m. If the data below $H_b = 440$ A/m are included in the fit, the resultant function does not correctly reproduce the data over the entire range of H_b.

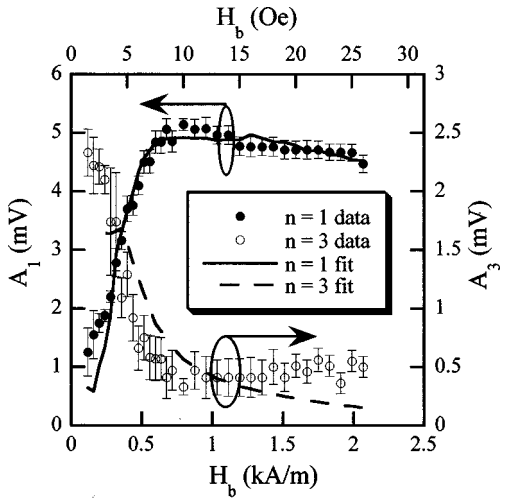

FIG. 6. Amplitudes of the $n=1$ mode A_1 and $n=3$ mode A_3 as a function of bias field. The data are fitted with a model described in Sec IV.

The relative amplitudes of the $n=1$ and $n=3$ spectral peaks do not remain constant with changing bias field, as may be seen in Fig. 6, where we show the relative amplitudes of the $n=1$ and $n=3$ peaks as obtained by fitting the data to Lorentzian-shaped peaks. The $n=3$ peak grows in amplitude with a reduction in H_b, whereas the $n=1$ peak shrinks.

In the case of step excitation, an accurate estimate for the pulsed field H_p is essential to properly fit the data: H_p affects both the equilibrium magnetization orientation and the precessional frequency. In the limit of no separation between the sample and waveguide, the pulsed field magnitude may be calculated from the voltage pulse amplitude using the characteristic impedance of the waveguide Z_0 and Ampere's law for a current sheet of width w.

$$H_p = \frac{V_p}{2Z_0 w}. \tag{16}$$

We assume V_p is equal to that produced by the pulse generator. For $w = 50\,\mu\mathrm{m}$, $V_p = 10\,\mathrm{V}$, and $Z_0 = 60\,\Omega$, we expect a pulse amplitude of 1.7 kA/m (21 Oe). We verified the validity of Eq. (16) by measuring the precessional frequency for a larger voltage pulse, employing a pulse generator capable of producing 40 V step wave forms, a factor of 4 greater than the pulse generator normally used for these measurements. We assume the majority of the sample magnetization was rotated by a full 90° under the influence of this large pulse. By measuring the precessional frequency, we calculate the field pulse amplitude by

$$\omega_p = \gamma\mu_0\sqrt{M_s(H_p - H_k)}. \tag{17}$$

The fits for $V_p = 10\,\mathrm{V}$ and $V_p = 40\,\mathrm{V}$ were corefined using Eqs. (12), (15), and (17) to determine self-consistent values for H_p, H_k, and g. We thereby determined that $H_p = 1.63\,\mathrm{kA/m}$ (20.4 Oe), only 3% less than predicted by Eq.

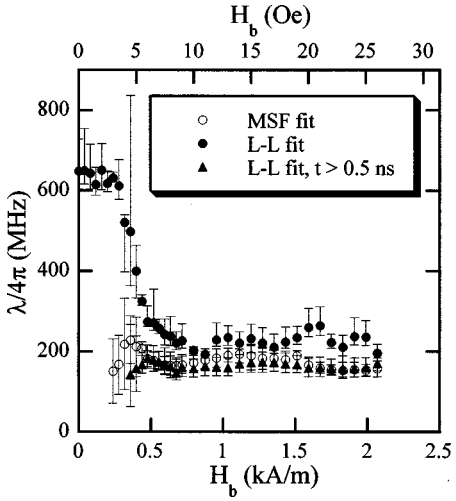

FIG. 7. LL damping for step-response data obtained by three different fitting methods. Open circles are the MSF results using Eq. (11). Filled circles are the result of fitting the entire time range of data to LL. Filled triangles are the result of fitting to LL, but over a restricted time range similar to that used for the MSF. The damping has been scaled by 4π to aid in comparison with past published values of $\lambda_{cgs}=\lambda/4\pi$.

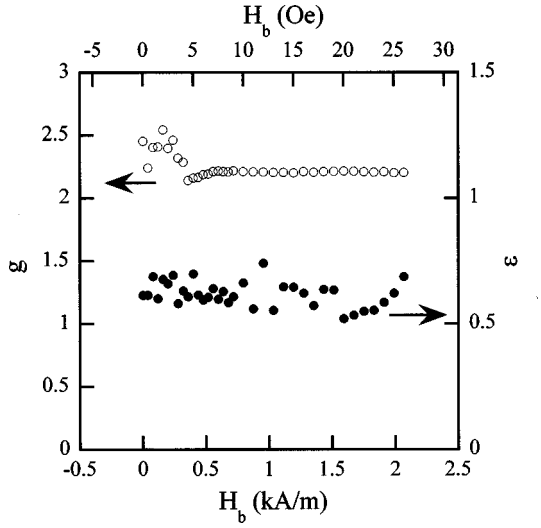

FIG. 8. Gyroscopic splitting factor g and inductive coupling efficiency ε resulting from fits of inductive step-response data to LL.

(16). Using fitted values for H_p and H_k, we infer an effective magnetization rotation angle for the case of zero bias field: $\phi_0=\arcsin(H_p/H_k)=63°$.

We extracted damping values from the step excitation data by three alternative methods. First, application of the MSF discussed previously yields the exponential damping time τ. Second, the data were fitted directly to the LL equation. The LL equation in spherical coordinates for a magnetic film in the xy plane may be written as

$$\frac{d\phi}{dt}=|\gamma|\mu_0 M_s\psi-\frac{\lambda}{\mu_0 M_s^2}\frac{\partial U}{\partial\phi},$$
$$\frac{d\psi}{dt}=\frac{|\gamma|}{M_s}\frac{\partial U}{\partial\phi}+\lambda\psi, \tag{18}$$

where ϕ is the azimuthal magnetization direction, ψ is the polar magnetization direction relative to the sample plane ($M_z=0$ for $\psi=0$), and we have assumed $\psi\ll 1$. Equation (18) is solved numerically, using the measured transmitted voltage pulse as the time dependent $H_p(t)$ in $\partial U/d\phi$. Only three free parameters were used to optimize the fit: γ, λ, and an inductive coupling efficiency ϵ. Finally, the data were fitted to a numerical solution of LL, but only over a reduced time range which excludes the first half cycle of oscillation in the inductive data. The results of all three methods are compared in Fig. 7. The damping obtained by the MSF and the numerical solution to LL over a restricted time range agree quite well within the experimental error. The average damping obtained by the MSF and the restricted numerical LL solution are $\lambda/4\pi=177\pm 20$ MHz and 164 ± 9 MHz, respectively. The damping obtained by numerical fitting of LL over the entire time range is in fair agreement with the other two methods, but only for $H_b\geqslant 0.7$ kA/m (9 Oe). For $H_b\geqslant 0.7$ kA/m, the average damping by full LL fitting is $\lambda/4\pi=225\pm 18$ MHz. For smaller bias fields, the full numerical solution yields a damping which rapidly increases with decreasing bias field. The damping saturates for $0<H_b<280$ A/m ($0<H_b<3.5$ Oe), with an average value of $\lambda/4\pi=634\pm 17$ MHz, roughly three times greater than the damping obtained for $H_b>0.7$ kA/m.

Fitting of the entire data set to LL also yields values for g and ϵ, the inductive coupling efficiency. Both g and the ϵ are plotted in Fig. 8. The average value for ϵ is 0.62 ± 0.05. The fitted value for g is constant only for $H_b>560$ A/m, where it is equal to 2.21. It varies between 2.14 and 2.55 below 560 A/m. This fitted value for g over the restricted range of H_b is in excellent agreement with that obtained by fitting the precessional frequencies to Eq. (12).

Mallinson and others have argued that the LL model for magnetodynamics is unphysical for large damping, in which case the Landau–Lifshitz–Gilbert model is more appropriate.[18] However, these two models are degenerate for the case of weak damping, $\alpha=\lambda/\gamma\mu_0 M\ll 1$.[19] The largest damping we observe is for $H_b\leqslant 280$ A/m (3.5 Oe), where $\lambda/4\pi<700$ MHz ($\alpha=0.05$). We thus conclude that the LL formalism is an appropriate model for the analysis of all our data.

Finally, a small digression into the assumption of in-plane sensitivity for this inductive technique is in order. We have assumed until now that the magnetization response is predominantly in-plane. However, the precessional motion of the magnetization as indicated by our data implies a nonzero perpendicular magnetization component. It is therefore reasonable to expect oscillations in the z component of magnetization to make a contribution to the total inductive signal. We do not believe these contributions to be of any significance for the experimental geometries employed by us. First, the out-of-plane sensitivity of the waveguide for an inductive signal has odd parity across the width of the waveguide (using the Karlqvist equations).[8] Thus, the waveguide cannot pick up the perpendicular component of even parity modes ($n=1,3,5,\ldots$). Second, the precessional motion of the magnetization is extremely elliptical, in virtue of the large difference between the out-of-plane and in-plane

anisotropies. The ratio of M_z to M_y for FMR excitations scales with the square root of the ratio of the in-plane and out-of-plane anisotropies:[20] $\sqrt{H_k/M_s} \approx 0.05$ for our samples. Thus, in the event that odd parity modes are present, the strength of the inductive signal due to the perpendicular magnetization component would be only 5% of the longitudinal magnetization signal strength, making them difficult to detect. We conclude that our assumption of negligible out-of-plane sensitivity, while an approximation, is justified.

IV. DISCUSSION

The presence of multiple peaks in the FFT spectra of step excitation data suggests that the magnetization reacts inhomogeneously to the application of the field step. While some microscopic inhomogeneity may be present (as ripple or defects), the fact that the samples are narrow enough in width to cause a significant increase in shape anisotropy suggests that finite size presents the largest source of inhomogeneity. We expect that the strong demagnetizing fields at the edges of the sample effectively pin the magnetization. Within the constraint of such a boundary condition, multiple odd-indexed excitation modes should be present, each with a well-defined eigenmode frequency of precession. Previous theoretical work by Bryant and co-workers treats the problem of finite Permalloy stripes for the case of FMR by numerically calculating the exact eigenmodes.[21] In the absence of an alternative theory, we shall compare our results to Bryant's theory.

We shall also discuss the peculiar nature of damping for step excitation data. Our results suggest that a more complex time-dependant damping may be required to provide a phenomenological description of our data. In addition, a correlation of the damping and $n=3$ mode amplitude provides strong evidence that the inhomogeneity responsible for the creation of higher-order excitation modes is also responsible for the strong increase in damping at low bias fields.

A. Anisotropy

The difference between the static, measured crystalline anisotropy and the fitted, dynamical H_k may be attributed to shape anisotropy. In the static case, the shape anisotropy of a finite width strip is not a well-defined quantity. Only ellipsoids have well-defined demagnetizing factors such that a uniform magnetization will result in a uniform demagnetizing field. Indeed, the static equilibrium distribution of $M(y)$ for a stripe is distinctly nonuniform for $H_p \neq 0$ in the limit of negligible crystalline anisotropy, whereas the demagnetizing field is uniform, with $H_d = -H_p$.[22] (This is a consequence of the requirement that the local torque be zero when **M** is in equilibrium.)

However, the dynamical case is different: The magnetization distribution may now fall into eigenmodes of precession, where a given eigenmode is defined as having a uniform precessional frequency everywhere in the sample. Presumably there is no single eigenmode solution, so we shall consider any particular nth eigenmode. Examination of Eq. (12) allows us to conclude that the total stiffness field H_{eff} must be uniform throughout the sample for any given eigenmode.

Let us consider only the shape anisotropy term in the local free energy of the sample:

$$U_k^s(y) = -\frac{\mu_0}{2} M_y(y) H_d(y). \tag{19}$$

As a first order approximation to a precessional eigenmode, let us presume that the *local* demagnetizing field $H_d(y)$ is proportional to the *local* magnetization $M_y^n(y)$ of the nth eigenmode through a demagnetizing factor N_n such that

$$H_d^n(y) = -N_n M_y^n(y). \tag{20}$$

The local free energy is therefore

$$U_k^s(y) = \frac{\mu_0}{2} N_n M_s^2 \sin^2 \phi(y). \tag{21}$$

The stiffness field, which determines the frequency of precession, is

$$\frac{\partial^2 U_k^s}{\partial \phi^2} \approx \mu_0 N_n M_s^2 = \mu_0 H_k^s(n) M_s, \tag{22}$$

where we have assumed that $\phi(y) \ll 1$ (that is, large bias fields) and have used the conventional definition of the shape anisotropy field, $H_k^s(n) \doteq N_n M_s$. Thus, we see that the dynamical shape-induced anisotropy field $H_k^s(n)$ represents the proportionality between the local magnetization of the nth eigenfunction solution $M_y^n(y)$ in the transverse direction and the local demagnetizing field $H_d^n(y)$, where

$$H_k^s(n) = \frac{H_d^n(y)}{M_y^n(y)} M_s. \tag{23}$$

$H_k^s(n)$ is approximately independent of position, thus satisfying the requirement that the entire eigenfunction precesses at the same frequency. (For arbitrary ϕ, the general requirement for an eigenfunction is that $\partial^2 U/\partial \phi^2$ be independent of position. This is a significantly more difficult theoretical problem to solve.) The magnitude of $H_k^s(n)$ will depend quantitatively on the exact functional form of the magnetization distribution $M_y^n(y)$. In the case of an infinite plane with the average magnetization aligned along the x axis, the magnetization profile is sinusoidal and the anisotropy is proportional to the wave number k_y^n (in the thin-sample limit, or $k_y^n \delta \ll 1$):[21]

$$H_k^s(n) = \tfrac{1}{2} k_y^n M_s \delta. \tag{24}$$

Pinning of the magnetization at $y = -w/2$ and $+w/2$ leads to a quantization of the wave number $k_y^n = n\pi/w$. For a finite width stripe, the wave number is further modified by edge effects due to the abrupt end of the magnetization at $\pm w/2$.[21] The effective mode number n_{eff} is defined as the normalized wave number $n_{\text{eff}} = k_y^n w/\pi$. Thus, an exact value for n_{eff} will also depend quantitatively on the functional form of $M_y^n(y)$. Bryant *et al.* calculated that, in the limit of uniform magnetization along the stripe length ($k_x = 0$), $n_{\text{eff}} = 0.735$ for k_y^1.[21] However, $n_{\text{eff}} \to 1$ as $k_x \to \infty$ ($n_{\text{eff}} \approx 1$ for $k_x \geqslant 20/w$, or $\lambda_x \leqslant 3.2/w$).[21]

The total anisotropy H_k is the sum of shape and crystalline components: $H_k = H_k^s(n) + H_k^{\text{xtal}}$. Since we have fitted dynamical anisotropies for two widths of sample stripes, we may then determine both n_{eff} and H_k^{xtal} in a simple algebraic fashion: $H_k^s(n)$ is inversely proportional to w, whereas H_k^{xtal} is not. If we use the anisotropy for the step response measurement as determined by the MSF, we have $n_{\text{eff}} = 1.45 \pm 0.09$ and $H_k^{\text{xtal}} = 160 \pm 60$ A/m (2 ± 0.8 Oe). Here, the crystalline anisotropy is in poor agreement with the statically measured value of 340 A/m (4.3 Oe). If instead we use the anisotropy for the step response measurement as determined by fitting to FFT spectra, we have $n_{\text{eff}} = 1.06 \pm 0.09$ and $H_k^{\text{xtal}} = 416 \pm 60$ A/m (5.2 ± 0.8 Oe). The crystalline anisotropy is now in good agreement with the statically measured value.

Note that the fitted n_{eff} is 1.5–2 times the theoretical value from Bryant *et al.* This disparity in n_{eff} is not yet understood. One possibility is that $k_x \neq 0$; that is, M is inhomogeneous in the direction parallel to the sample stripe. Also, Bryant *et al.* considered only the case of a large external bias field $H_b \gg H_k^{\text{xtal}}$ such that $\phi_0 = 0$.[21] It is conceivable that the eigenfunctions $M_y^n(y)$ are significantly altered for $\phi_0 \neq 0$ and $H_k^{\text{xtal}} \neq 0$.

B. Signal amplitude

We expect the magnetization rotation for our samples to be nonuniform, as determined by the spatial profile of the excited dynamical eigenmodes. If the magnetization rotation were uniform, we would predict a theoretical magnetization change of

$$M_y^{\text{th}} = M_s \sin \phi, \tag{25}$$

where ϕ is determined for step data from Eq. (15). We define the normalized experimental coupling efficiency as $\epsilon = \overline{M_y}/M_y^{\text{th}}$, using Eq. (5) to determine $\overline{M_y}$. As such, ϵ is a quantitative measure of the nonuniformity inherent in the magnetization rotation. Numerical fitting of the step-response data to LL yields $\epsilon = 0.78 \pm 0.06$.

We consider the equilibrium magnetization profile long after application of the field step for $H_b = 0$. The magnetization distribution as a function of position y across the width of the sample is given by[22]

$$M_y(y) = \frac{H_p w}{\delta} \sqrt{1 - \left(\frac{2y}{w} - 1\right)^2}, \tag{26}$$

where $0 < y < w$. The derivation of Eq. (26) ignores any crystalline anisotropy and assumes $\delta/w \ll 1$. The average of Eq. (26) across the width of the sample is

$$\overline{M_y} = \frac{\pi}{4}\left(\frac{H_p w}{\delta}\right). \tag{27}$$

Bryant *et al.* predict the dynamical shape anisotropy given by Eq. (24), where they, like Bertram, also ignore crystalline anisotropy. If we were to naively assume uniform behavior when predicting magnetic rotation, as is assumed for Eq. (25), then we would conclude

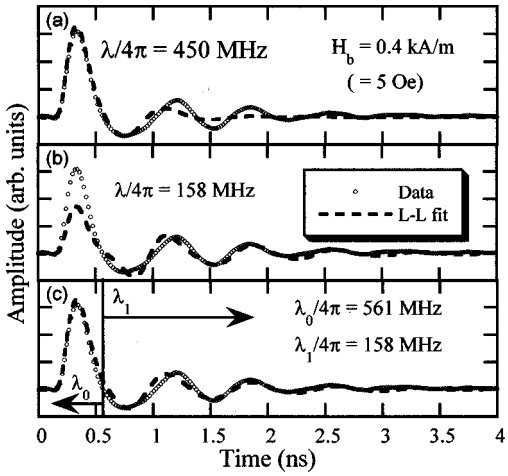

FIG. 9. Results of fitting inductive step-response data for $H_b = 0.4$ kA/m (5 Oe) using LL. (a) The result of a fit when only the first ~ 0.5 ns of data is used for the fitting with a fitted damping of $\lambda/4\pi = 450$ MHz. (b) The result of a fit when the last 3.5 ns of data is used for the fitting with a fitted damping of $\lambda/4\pi = 158$ MHz. (c) Demonstrates a fit to the data using a model of time-varying damping, with fitted damping of $\lambda_0/4\pi = 561$ MHz and $\lambda_1/4\pi = 158$ MHz.

$$M_y = M_s \frac{H_p}{H_k^n} \tag{28}$$

$$= \frac{2}{n_{\text{eff}}\pi}\left(\frac{H_p w}{\delta}\right). \tag{29}$$

We then estimate ϵ as the ratio of Eqs. (27) and (28). Using Bryant's calculated value of $n_{\text{eff}} = 0.735$ for the lowest-order mode with $k_x = 0$, we arrive at $\epsilon = n_{\text{eff}}\pi^2/8 \approx 0.91$, in fair agreement with the experimentally derived value. A more accurate calculation would consider static and dynamic magnetization profiles with $H_k^{\text{xtal}} \neq 0$ and $\phi_0 \neq 0$.

C. Damping

The damping has a different dependence on bias field for the impulse and step response data. While the impulse data exhibit a slow monotonic increase in damping as the bias field is reduced, the step data are relatively constant for $H_b > 0.6$ kA/m (7.5 Oe), as obtained by our three different methods. For bias fields less than 0.6 kA/m, the damping is dramatically different, depending on whether the analysis includes or excludes the initial cycle of inductive oscillation. Including the initial portion of the wave form in the numerical fitting procedure results in a sharp increase in damping between $0.3 < H_b < 0.5$ kA/m, below which the damping is relatively constant, with $\lambda/4\pi = 650$ MHz. Exclusion of the initial 1–2 cycles of oscillation produces damping values which remain unchanged with bias field. These disparate values for fitted damping, depending on the temporal range of fitted data, suggest that the damping is not constant over the entire time range of measurement. This notion is exemplified in Fig. 9, where several attempts to fit $H_b = 0.4$ kA/m (5 Oe) step response data are shown. Figure 9(a) compares the data and fit when the numerical algorithm is optimized to fit the first ~ 500 ps of inductive response. While the fit is good during the early portion of inductive response, it clearly suffers from overdamped behavior relative to the latter portion

of data. Figure 9(b) presents the converse situation, where the fitting algorithm was optimized for the all the data except the first nanosecond of response. Again, the fit is good over the optimized range of time, but fails to fit the first half cycle of oscillation by a factor of 2. It appears that there is a transient increase in damping during the early portion of dynamical response.

To test whether the notion of anomalous transient damping is a plausible explanation for the observed phenomena, we used the following model: The damping is set to an initial value λ_0 and is abruptly changed to a final value λ_1 at a time corresponding to a half period of oscillation in the experimental data. Again, the driving function used for the fit is derived from the measured voltage pulse transmitted through the waveguide. We fit the data with LL using four free parameters: λ_0, λ_1, γ, and ϵ. The resulting fit is shown in Fig. 9(c). The fit is now good over the entire time span of the data. Further, the fitted damping is almost a factor of 4 larger during the initial stage and is comparable to the damping obtained by fitting the entire wave form with a single damping parameter.

Admittedly, this step-function model is somewhat arbitrary, and we have chosen it for its numerical simplicity. A more accurate representation of time-dependent damping would presumably result in a more continuous variation of damping with time. However, we present this model as an elementary analysis to provide quantitative results based upon the observed phenomenology.

The large transient damping observed at low bias fields may explain the poor fit to Eqs. (12) and (15) of the $n=1$ FFT spectral peak in this field range. The $n=1$ peak data are redshifted at low bias fields compared to the fit. This anomalous spectral shift is absent in the precessional frequencies obtained by fitting the data to a modified damped sinusoid, which excludes the initial 1–2 cycles of magnetic response. The FFT result may represent a frequency shift resulting from a large initial stage of damping. We show in Appendix B the well-known result that damping shifts the resonance frequency of magnetic precession down from its asymptotic limit according to Eq. (A8). For $H_b=320$ A/m (4 Oe), the FFT-derived precession frequency is $f_p^{\mathrm{FFT}}=1.175$ GHz. The LL derived damping is $\lambda^{\mathrm{LL}}/4\pi=521$ MHz. In the limit of linear oscillatory analysis, we expect the ''ideal'' (free of damping) precession frequency to be $f_0=[(f_p^{\mathrm{FFT}})^2-(\lambda^{\mathrm{LL}})^2]^{1/2}=1.285$ GHz, implying a damping-induced frequency shift of 110 MHz. This frequency shift is close to the measured error of 128 MHz between the precessional frequency data and the fit to Eqs. (12) and (15) at $H_b=320$ A/m (4 Oe). While such analysis shows that the damping obtained by the LL fitting is a plausible explanation for the anomalous frequency shift observed for the $n=1$ peak, a more complete quantitative analysis is difficult, due to the nonlinear nature of magnetization dynamics when the magnetization is driven over large excursion angles.

D. Spectra

The occurrence of multiple spectral peaks for step-response excitations, indicating multiple precessional modes, distinguishes the step response from impulse response and greatly complicates the analysis of the step data. Indeed, using LL to fit the data is clearly suspect for $H_b<0.28$ kA/m (3.5 Oe), where the $n=3$ peak exceeds the $n=1$ peak in magnitude. This may partly explain why the fitted values for g shown in Fig. 8 become less stable for $H_b<0.28$ kA/m (3.5 Oe). Clearly, the simple picture of coherent magnetic precession is inappropriate at low bias fields.

One possible explanation for the growth of the $n=3$ mode at low bias fields is the saturation of the $n=1$ mode for large ϕ_0. Such a saturation may be described by a purely geometrical formulation, which naturally leads to nonlinear effects. We begin by assuming that the magnetization is originally excited in the $n=1$ mode, characterized by a sinusoidal distribution of the magnetization angle across the width of the waveguide:

$$\phi(y,t)=g(t)\sin\left(\frac{\pi y}{w}\right), \tag{30}$$

where $0<y<w$ and $g(t)$ is the time-dependent amplitude for the excitation. We ignore finite size effects since these generally act as perturbations to the classical magnetostatic mode result of Damon and Eshbach.[21] We expect to couple preferentially to the $n=1$ mode since the excitation field is approximately uniform across the sample width. The magnetization in the transverse direction is given by

$$\begin{aligned} M_y &= \sin[\phi(y,t)] \\ &= 2J_1[g(t)]\sin\left(\frac{\pi y}{w}\right)+2J_3[g(t)]\sin\left(\frac{3\pi y}{w}\right)+\cdots. \end{aligned} \tag{31}$$

Thus, we see that large magnetization rotations will naturally spawn higher-order spatial modes. Note the dependence of the respective amplitudes upon Bessel functions, with the excitation amplitude as arguments. Such a nonlinear mechanism will depend primarily upon the maximum excursion angle $\phi_{\max}$ of the magnetization immediately following application of the field step. In the limit of negligible damping, we may numerically solve for $\phi_{\max}$ using

$$U(\phi=0)=U(\phi_{\max}), \tag{32}$$

where $U(\phi)$ is the free energy of the magnetic sample after the field step has settled to the equilibrium value of H_p, and we are equating the energy at the moment **M** begins to move and when **M** reaches it maximum angle. We may now model the amplitudes of the $n=1$ and $n=3$ spectral peaks (A_1 and A_3, respectively) as

$$\begin{aligned} A_1 &= C_1 J_1[\phi_{\max}(H_b)] f_p(n=1), \\ A_3 &= C_2 J_3[\phi_{\max}(H_b)] f_p(n=3), \end{aligned} \tag{33}$$

where we have scaled the amplitudes by the precessional frequencies of the two different modes to account for the inductive method of detection [see Eq. (4)]. The inset to Fig. 6 shows the results of fitting the spectral amplitude data to Eq. (33), with only C_1 and C_2 as fitting parameters. The model fits the spectral dependence for the $n=1$ mode on H_b accurately, including the occurrence of a cusp in the $n=1$ data around 0.6 kA/m (7.5 Oe). The fit for the $n=3$ mode is in more qualitative agreement, where both the model and data display a rapid increase in the amplitude of the $n=3$ mode for $H_b<0.8$ kA/m (10 Oe). However, the model pre-

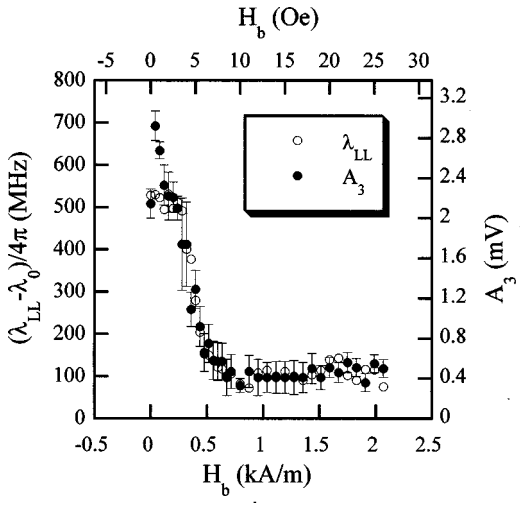

FIG. 10. Comparison of damping obtained via fitting to LL λ_{LL} and the amplitude of the $n=3$ peak A_3 vs H_b. The damping data are shifted down by $\lambda_0=121$ MHz to account for intrinsic damping mechanisms, which should not affect the amplitude of the $n=3$ mode.

dicts a monotonic decrease in the amplitude of the $n=3$ peak with increasing H_b, in contrast to the data, which settle to an asymptotic value of 0.4 ± 0.1 mV for $H_b>0.8$ kA/m (10 Oe).

This saturation-induced nonlinear mechanism for the generation of higher-order precessional modes may partly explain the time-variant damping discussed above. Indeed, the damping obtained by fitting the step-response data to LL and the amplitude of the $n=3$ peak obtained by Fourier transformation have similar dependences on bias field, as shown in Fig. 10. This similarity supports the notion that saturation-induced mode generation is the source of anomalous transient damping seen in our data.

Sandler and Bertram have performed micromagnetic simulations for a magnetic system modeled after the inductive experiments presented here.[23] They have observed an inhomogeneous magnetization distribution during the reversal process with clear indications that higher order spatial modes are indeed present. In addition, they find that their simulations can reproduce the phenomenology of the transient damping process observed in our experiments, although the micromagnetic simulation employs only a fixed microscopic damping constant. Presumably, a microscopically defined damping parameter is a reasonable approximation to the intrinsic damping. We conclude that the damping parameter which we fit to the data is an effective value for damping, not to be confused with an intrinsic damping parameter. While the intrinsic damping is representative of the fundamental physical coupling between magnetic excitations and the crystalline lattice through magnon–phonon scattering processes, an effective damping includes less intrinsic effects such as inhomogeneous broadening and nonlinear mode conversion (i.e., magnon–magnon scattering). A comparison of damping parameters obtained by micromagnetic modeling and phenomenological fitting should shed light on the degree of nonintrinsic effects present in our experimental system.

V. CONCLUSION

While the understanding of precessional processes in ferromagnetic materials has been greatly advanced by FMR over the past five decades, a lack of time-domain data to facilitate a similar understanding of fundamental limits to switching speeds in technologically relevant materials remains. The dearth of time-resolved data has partly stemmed from the lack of a simple and direct method for such measurements. The inductive method described here is both simple and direct, albeit the analysis of the data may be complex. The complexity of the analysis is in part due to the lack of appropriate theoretical tools for the understanding of switching dynamics under the influence of moderately large field pulses. Indeed, we have found several phenomena (saturation-induced nonlinear mode generation, transient damping) through the analysis of our data which appear unique to time-resolved experimentation. Nevertheless, a conventional analysis based upon the Landau–Lifshitz equation can provide a coarse understanding of the dynamical processes with some degree of quantitative self-consistency.

Alternative methods for time-resolved observation of subnanosecond magnetization dynamics have been developed in recent years. Time-resolved Kerr microscopy has successfully resolved precessional dynamics in both YIG and Permalloy films.[24,25] One obvious advantage of such an optical method is the capability to spatially resolve details of nonuniform dynamics. Recent efforts to use pulsed x-ray sources for time-resolved spin polarized photoemission measurements have been fruitful.[26] However, both such techniques are expensive and complex to implement. The inductive method presented here is much simpler, both in design and in use, with the exception of our use of a mode-locked Ti:sapphire laser as part of the impulse generator. We used a femtosecond laser due to its timely availability; there exist commercial electronic sources for impulse generators which are easier to both acquire and operate.

Three different analyses are used to extract gyromagnetic parameters for step excitations from our samples. The use of multiple fits was necessitated by our inability to fit the data with any one approach to a high degree of certainty. The MSF technique provided precessional frequencies as a function of bias field which may then be fitted with the standard equations for ferromagnetic resonance. It also provides a damping value which describes the rate of the exponential decay long after the application of the field step. In essence, the MSF approach bridges the gap between our time-resolved data and a conventional, pulsed FMR measurement. Use of LL to fit our data is justified only if all the magnetization in the sample precesses at the same frequency as a well-defined eigenmode. The observation of higher-order modes through FFT analysis should preclude LL fitting. However, such analysis is instructive as to the degree to which our sample departs from a simple, uniform model of precession with reduced bias field. Finally, a comparison of the LL fits restricted to long times after the field step and the MSF results serve dual purposes: verification of the approximations used to derive the MSF algorithms, and clarification that any departure of our data from ideal LL behavior appears localized in time to the early stages of gyromagnetic response.

This technique is by no means limited to the sample parameters presented. It is general in its applicability to a wide spectrum of soft ferromagnetic materials and sample geometries. In addition, this technique lends itself to comparative studies by alternative laboratory methods, such as Kerr microscopy, time-resolved optical methods, and scanned probe microscopies such as magnetic force microscopy.

In summary, we have presented detailed results from a new inductive method for characterizing magnetization dynamics. This work builds upon previous implementations of inductive techniques by employing modern high-speed sampling technology, lithographic waveguide fabrication, and digital signal processing. We have demonstrated its use in structures with a 3 GHz bandwidth, although our sampling oscilloscope's temporal resolution would easily permit measurements over an 18 GHz bandwidth. For Permalloy, we measured switching times as short as 200 ps for an inferred 60° rotation. Shape-induced demagnetization strongly affects the magnetization oscillation frequency. Anomalous behavior was found for step-response experiments when the bias field was reduced below 640 A/m (8 Oe), including the growth of higher-order precessional modes and transient damping. Both phenomena may be partly explained in terms of nonuniform magnetization dynamics.

ACKNOWLEDGMENTS

Early conversations with Mark Freeman were a source of inspiration for the authors to pursue studies of magnetodynamics. The authors acknowledge helpful discussions with Pavel Kabos and Bob McMichael, both of whom guided them to an understanding of modal analysis for ferromagnetic resonance. John Mallinson helped clarify salient distinctions between the Landau–Lifshitz and Landau–Lifshitz–Gilbert equations. Ron Goldfarb provided useful comments on the manuscript and contribution to Appendix A. They are grateful for the assistance of Don DeGroot in measuring the bandwidth of our devices. Tony Kos provided invaluable engineering assistance with the experimental details of the step excitation measurements.

APPENDIX A

The Landau–Lifshitz equation in two systems of units is

$$\frac{d\mathbf{M}}{dt} = -|\gamma|\mathbf{T} - \frac{\lambda}{\mu_0 M_s^2}(\mathbf{M}\times\mathbf{T})(\text{SI units}), \tag{A1}$$

$$\frac{d\mathbf{M}}{dt} = -|\gamma|\mathbf{T} - \frac{\lambda}{4\pi M_s^2}(\mathbf{M}\times\mathbf{T})(\text{cgs units}), \tag{A2}$$

where M in Eq. (A2) has units of $\text{erg Oe}^{-1}\,\text{cm}^{-3} \equiv \text{emu cm}^{-3}$. The damping parameter λ is in units of s^{-1} and is numerically identical in either system. This is not the same definition for LL damping historically invoked by either Smith or Wolf.[4,11] We shall call their previous definition of damping λ_{cgs}, and the relationship between damping parameters is $\lambda = 4\pi\lambda_{\text{cgs}}$. The factor of 4π in Eq. (A2) is required for dimensional balance.

The torque $\mathbf{T}$ in spherical coordinates is

$$\mathbf{T} = \frac{1}{\sin(\theta)}\frac{\partial U}{\partial \phi}\hat{\theta} - \frac{\partial U}{\partial \theta}\hat{\phi}, \tag{A3}$$

where $U(\theta,\phi)$ is the free energy *density* of the system. Under the approximations $M_s \gg H_k$ (''soft'' ferromagnet) and $\lambda \ll \gamma 4\pi M_s$ (''underdamped'' oscillator), the Landau–Lifshitz equation may be reduced to[11]

$$\frac{d^2\phi}{dt^2} + \lambda\frac{d\phi}{dt} + \mu_0\gamma^2\frac{\partial U}{\partial \phi} = 0. \tag{A4}$$

A field step is applied at $t=0$, which shifts the magnetization equilibrium direction from $\phi = 0$ to ϕ_0. For small motion of ϕ, we may expand $\partial U/\partial\phi$ in a Taylor series and further approximate Eq. (A4) as

$$\frac{d^2\phi}{dt^2} + \lambda\frac{d\phi}{dt} + \mu_0\gamma^2\left(\frac{\partial^2 U}{\partial \phi^2}\right)_{\phi_0}[\phi - \phi_0 u(t)] = 0, \tag{A5}$$

where $u(t)$ is the Heaviside step function. Taking a Laplace transform of Eq. (A5) and setting the initial conditions to $\phi(0) = 0$ and $\phi'(0) = 0$, we have

$$s^2\Phi + \lambda s\Phi + \omega_0^2\Phi = \frac{\omega_0^2\phi_0}{s}, \tag{A6}$$

where $\omega_0^2 = \mu_0\gamma^2(\partial^2 U/\partial\phi^2)_{\phi_0}$. Solving for Φ, we find

$$\Phi \approx \phi_0\left[\frac{1}{s} - \frac{s+\lambda/2}{(s+\lambda/2)^2+\omega_p^2} - \left(\frac{\lambda}{2\omega_p}\right)\frac{\omega_p}{(s+\lambda/2)^2+\omega_p^2}\right], \tag{A7}$$

where

$$\omega_p^2 = \omega_0^2 - (\lambda/2)^2. \tag{A8}$$

Taking the inverse Laplace transform, we find

$$\phi(t) = \phi_0\left\{1 - e^{-t/\tau}\left[\cos(\omega_p t) - \left(\frac{1}{\tau\omega_p}\right)\sin(\omega_p t)\right]\right\}u(t), \tag{A9}$$

where $\tau = 2/\lambda$.

Thus, the solution is an exponentially damped sinusoid, even in the case of a step excitation. However, the magnetization angle now oscillates about the new equilibrium magnetization angle ϕ_0, as determined by a solution to Eq. (15). Since actual excitation sources produce pulses which deviate somewhat from a perfect step, we may generalize our solution to the form

$$\phi(t) = \phi_0 + \beta_0 e^{-t/\tau}\sin(\omega_p t + \varphi), \tag{A10}$$

where $\tau = 2/\lambda$, β_0 and φ are fitted parameters, and sufficient time has elapsed such that the applied field step has attained a final value.

APPENDIX B

The inductive voltage is given by Eq. (4). We shall assume $\varphi = 0$, without loss of generality. Since the geometry employed by the described technique detects changes in the flux along the y axis only, then the detected component of magnetization is given by

$$
\begin{aligned}
M_y &= M_s \sin[\phi(t)] \\
&= M_s \sin[\phi_0 + \beta_0 e^{-t/\tau} \sin(\omega_p t)] \\
&= M_s \{\sin(\phi_0)\cos[\beta_0 e^{-t/\tau}\sin(\omega_p t)] + \cos(\phi_0)\sin[\beta_0 e^{-t/\tau}\sin(\omega_p t)]\} \\
&= M_s \left\{ \begin{array}{l} \sin(\phi_0)\left[J_0(\beta_0 e^{-t/\tau}) + \sum\limits_{n=2,4,6,\ldots}^{\infty} 2J_n(\beta_0 e^{-t/\tau})\cos(n\omega_p t) \right] \\ +\cos(\phi_0) \sum\limits_{n=1,3,5,\ldots}^{\infty} 2J_n(\beta_0 e^{-t/\tau})\sin(n\omega_p t) \end{array} \right\},
\end{aligned} \tag{B1}
$$

where $J_n(x)$ is the nth Bessel function. When the magnetization precession angle has become sufficiently small such that $\beta_0 e^{-t/\tau} \ll 1$, we may use the asymptotic form of the Bessel function with the result

$$
\begin{aligned}
M_y &\approx M_s \left\{ \begin{array}{l} \sin(\phi_0)\left[1 + \sum\limits_{n=2,4,6,\ldots}^{\infty} \frac{2}{n!}\left(\frac{\beta_0 e^{-t/\tau}}{2}\right)^n \cos(n\omega_p t) \right] \\ +\cos(\phi_0) \sum\limits_{n=1,3,5,\ldots}^{\infty} \frac{2}{n!}\left(\frac{\beta_0 e^{-t/\tau}}{2}\right)^n \sin(n\omega_p t) \end{array} \right\} \\
&\approx M_s \left\{ \begin{array}{c} \sin(\phi_0)\left[1 + \frac{\beta_0^2}{4} e^{-2t/\tau}\cos(2\omega_p t) \right] \\ +\cos(\phi_0)\left[\beta_0 e^{-t/\tau}\sin(\omega_p t) + \frac{\beta_0^3}{24} e^{-3t/\tau}\sin(3\omega_p t) \right] \end{array} \right\},
\end{aligned} \tag{B2}
$$

retaining terms up to third order in β_0. Taking a time derivative and using the ''underdamped'' oscillator approximation $\omega_p \tau \gg 1$,

$$
\frac{dM_y}{dt} \approx \omega_p M_s \left[\begin{array}{c} \cos(\phi_0)\beta_0 e^{-t/\tau}\cos(\omega_p t) + \sin(\phi_0)\frac{\beta_0^2}{2} e^{-2t/\tau}\sin(2\omega_p t) \\ +\cos(\phi_0)\frac{\beta_0^3}{8} e^{-3t/\tau}\cos(3\omega_p t) \end{array} \right]. \tag{B3}
$$

The third harmonic distortion, represented by the third term in Eq. (B3), will always be very small compared to the fundamental frequency, no matter what the value for ϕ_0 is. However, the SHD may become arbitrarily large relative to the fundamental as ϕ_0 approaches $\pi/2$. Thus, we have our final form

$$
\begin{aligned}
\frac{dM_y}{dt} &\approx \omega_p M_s [\cos(\phi_0)\beta_0 e^{-t/\tau}\cos(\omega_p t) \\
&\quad + \tfrac{1}{2}\sin(\phi_0)\beta_0^2 e^{-2t/\tau}\sin(2\omega_p t)].
\end{aligned} \tag{B4}
$$

The degree of SHD is given by the ratio of fundamental to second-harmonic signals

$$
\mathrm{SHD} = \tfrac{1}{2}\tan(\phi_0)\beta_0 e^{-t/\tau}.
$$

The distortion diminishes with time as the gyromagnetic precession damps out. If an acceptable level of distortion $\mathrm{SHD}_{\min}$ can be determined, then the time $t_{\min}$ required to wait until the wave form is well approximated by a simple, damped sinusoid is given by

$$
t_{\min} = -\tau \ln\left(\frac{2 \cdot \mathrm{SHD}_{\min}}{\beta_0 \tan\phi_0} \right).
$$

For the sake of example, let us suppose that a distortion of $\mathrm{SHD}_{\min} = 5\%$ is acceptable. Let us also suppose that $\beta_0 \approx \phi_0$, which is equivalent to assuming that the free energy profile $U(\phi)$ may be approximated by a parabola. Finally, let us assume a damping of $\lambda = 130\,\mathrm{MHz}$, a typical value for $Ni_{81}Fe_{19}$.[4] If the magnetization rotation is only $\phi_0 = 20°$, then the required waiting time for simple sinusoidal behavior is $t_{\min} = 0.2\tau = 250\,\mathrm{ps}$. However, if the magnetization rotation is as large as $\phi_0 = 60°$, then the wait time increases to $t_{\min} = 2.9\tau = 3.6\,\mathrm{ns}$. Such a long waiting time is prohibitive because the signal will have decayed to a level insufficient for numerical fitting, given the finite signal-to-noise ratio of the inductive measurement.

[1] K. B. Klaassen, R. G. Hirko, and J. T. Contreras, IEEE Trans. Magn. **34**, 1822 (1998).
[2] W. Dietrich, W. E. Proebster, and P. Wolf, IBM Journal , 189 (April 1960).
[3] W. Dietrich and W. E. Proebster, J. Appl. Phys. **31**, 281S (1960).
[4] P. Wolf, J. Appl. Phys. **32**, 95S (1961).
[5] R. K. Hoffmann and H. H. Howe, *Handbook of Microwave Integrated Circuits* (Artech House, Boston, MA, 1987), p. 359.
[6] A. Stankiewicz, W. K. Hiebert, G. E. Ballentine, K. W. Marsh, and M. R. Freeman, IEEE Trans. Magn. **34**, 1003 (1998).
[7] J. C. Mallinson, *The Foundations of Magnetic Recording*, 2nd ed. (Academic, San Diego, CA, 1993), p. 92.
[8] H. N. Bertram, *Theory of Magnetic Recording* (Cambridge University Press, Cambridge, 1994), p. 59.
[9] J. C. Mallinson, in Ref. 7, p. 51.
[10] H. N. Bertram, in Ref. 8, p. 112.

[11] D. O. Smith, J. Appl. Phys. **29**, 264 (1958).
[12] Charles Kittel, *Introduction to Solid State Physics*, 6th ed. (Wiley, New York, 1986), p. 480.
[13] M. H. Seavey, Jr., and P. E. Tannenwald, J. Appl. Phys. **29**, 292 (1958).
[14] Z. Celinski and B. Heinrich, J. Appl. Phys. **70**, 5935 (1991).
[15] F. Vescial, T. J. Hutchings, E. D. Jacobs, and W. L. Zingery, J. Appl. Phys. **36**, 1054 (1965).
[16] D. O. Smith and K. J. Harte, J. Appl. Phys. **33**, 1399 (1962).
[17] E. C. Stoner and E. P. Wohlfarth, Philos. Trans. R. Soc. London, Ser. A **240**, 599 (1948).
[18] J. C. Mallinson, IEEE Trans. Magn. **23**, 2003 (1987).
[19] H. B. Callen, J. Phys. Chem. Solids **4**, 256 (1958).
[20] C. Vittoria, *Microwave Properties of Magnetic Films* (World Scientific, Singapore, 1993), p. 109.
[21] P. H. Bryant, J. F. Smyth, S. Schultz, and D. R. Fredkin, Phys. Rev. B **47**, 11255 (1993).
[22] H. N. Bertram, in Ref. 8, p. 176.
[23] G. Sandler, H. Neal Bertram, T. J. Silva, and T. M. Crawford, J. Appl. Phys. **85**, 5080 (1999).
[24] M. R. Freeman, M. J. Brady, and J. Smyth, Appl. Phys. Lett. **60**, 2555 (1992).
[25] W. K. Hiebert, A. Stankiewicz, and M. R. Freeman, Phys. Rev. Lett. **79**, 1134 (1997).
[26] F. Sirotti, R. Bosshard, P. Prieto, G. Panaccione, L. Floreano, A. Jucha, J. D. Bellier, and G. Rossi, J. Appl. Phys. **83**, 1563 (1998).